

OPTIMIZATION OF A NOVEL RBCC PROPULSION SYSTEM BY GENETIC ALGORITHM

Greg Chorkawy*, J. Etele**

*(gchorkaw@connect.carleton.ca), **(jetele@mae.carleton.ca)

**Department of Mechanical and Aerospace Engineering, Carleton University,
1125 Colonel By Drive, Ottawa, ON, K1S5B6, Canada**

Keywords: *Ejector, RBCC, Genetic Algorithm, Optimization*

Abstract

An interesting area of research in propulsion systems is rocket-based combined-cycle systems. This paper presents the implementation of a genetic algorithm to optimize the geometric configuration of a novel ejector nozzle for a rocket-based combined-cycle propulsion system. The genetic algorithm uses an adaptive technique that shows better performance when compared with standard techniques. The algorithm allows the user to easily adjust the fitness function to optimize for one or a combination of the following criteria: air intake area, flow turning angle, and shear layer mixing area. The optimized ejector nozzle shows potential for high entrainment of atmospheric air and thorough mixing of the air and rocket stream.

1 Introduction

An active area of research is the development of advanced space transportation technologies to allow more cost effective access to space. In order to reduce launch costs, more efficient propulsive systems are being considered. An approach that incorporates existing rocket technologies that can increase propulsive efficiency is a rocket-based combined-cycle (RBCC) propulsion system. A launch vehicle with this system will operate in four modes from lift-off to orbit: 1) rocket-ejector mode, Mach 0-3; 2) ramjet, Mach 3-7; 3) scramjet, Mach 7-12; 4) pure-rocket, Mach 12-

orbital velocity. A schematic diagram of a potential RBCC engine is shown in Fig. 1. This paper focuses on the rocket-ejector mode, which is an air-augmented rocket cycle. Atmospheric air is drawn into the engine to be mixed with the rocket stream, thereby increasing the mass flow through the system.

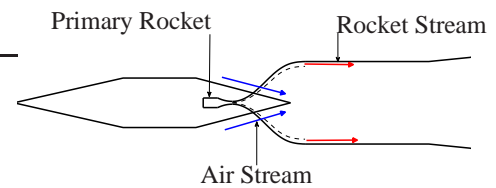


Fig. 1 Schematic Diagram Of A Potential RBCC Engine.

The performance of an RBCC engine is dependent on the quality of mixing and combustion of the atmospheric air stream and the rocket stream. Therefore, mixing configuration is a crucial matter. There are two general strategies for mixing: Diffusion and Afterburning (DAB), and Simultaneous Mixing and Combustion (SMC). In the DAB cycle, the inert rocket stream and atmospheric air stream are mixed and diffused, then fueled and burned subsonically in an afterburner. In the SMC cycle, fuel-rich rocket stream is continuously mixed and reacted with the air stream. DAB yields better performance than SMC at sea-level static conditions, however the performance converges with increasing altitude and flight speed [1]. The SMC cycle is less complex than the DAB cycle and requires a

shorter mixing duct, leading to lower structural weight.

Other mixing schemes have been considered. The Independent Ramjet Stream (IRS) cycle has been considered by NASA's GTX project [2, 3]. In this cycle, the air stream is fueled upstream and the rocket plume is used to ignite the fuel-air mixture. It has been found by Yungster and Treffny that at subsonic speeds the IRS cycle shows lower performance when compared with other RBCC engines schemes [4]. The Shielded Primary Injection (SPI) scheme, developed by Russell et al [5], is a combination of SMC and DAB cycles. Fuel is injected upstream in the inert rocket stream and is shielded from the oxidizing air stream by the rocket stream. Russell et al have shown that SPI combines the advantages of DAB and SMC.

The rocket exhaust profile can affect mixing between rocket and air stream, which affects the efficiency of the RBCC engine. The Marquardt Corporation developed a correlation for mixing length as a function of several parameters, including the total number of thrusters in the duct; the relationship states that the mixing length is inversely proportional to the number of thrusters in the duct [6]. It has also been found that mixing performance improved when an annular rocket exhaust profile is used, allowing for shorter duct lengths [7]. To take advantage of shorter duct lengths while avoiding the use of multiple thrusters, a novel ejector concept that generates an annular rocket exhaust profile from a single circular throat has been developed [8]. The flow path of the supersonic portion of the nozzle is shown in Fig. 2 and 3. A design code was developed to generate the geometric configuration of this supersonic nozzle. The shape is calculated to yield a pre-specified Mach number distribution while passing through a "gate" (as shown in Fig. 2). The position and shape of the gate, defined by five geometric variables, are used to manipulate the geometry of the rocket flow path. A second design code is then used to generate the contour of the entrained air intake that surrounds the supersonic rocket flow path [9]. The air intake allows for entrainment of atmospheric

air while minimizing total pressure and mass flow rate losses. An exploded view of the combined design, shown in Fig. 4, consists of an axisymmetric center body, a cowl and nozzle fairings within which the rocket flow path is housed.

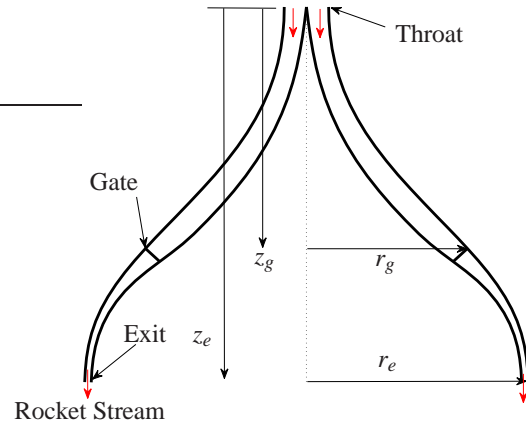


Fig. 2 Side View Of The Rocket Flow Path.

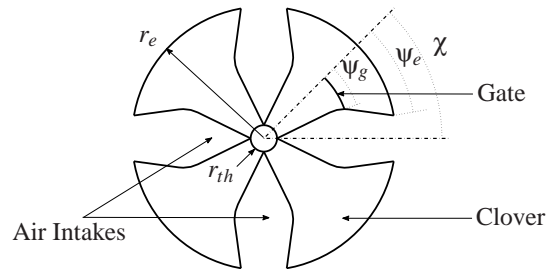


Fig. 3 Top View Of The Rocket Flow Path. The Dashed-Dot Lines Represent Half A Clover.

The purpose of this paper is to outline the implementation of a genetic algorithm (GA) to determine the optimal combination of rocket and air intake geometry such that pre-defined performance criteria are achieved. GAs are well established optimization techniques and have been widely used in engineering optimization problems [10, 11].

2 Implementation

2.1 Rocket Flow Path Geometry

The first step of the optimization process is to generate an optimal rocket flow path. The position and shape of the gate are used to manipulate the rocket flow path geometry. Fig. 2 and Fig. 3

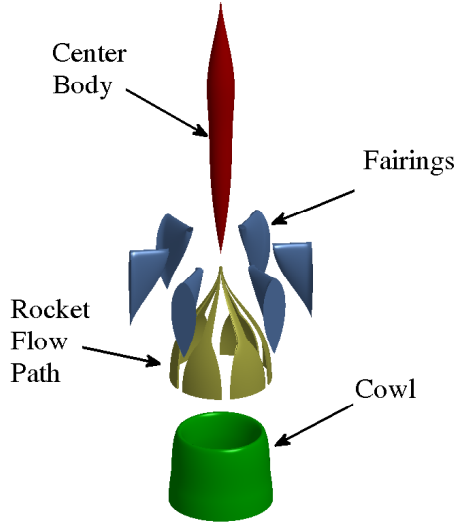


Fig. 4 Exploded View Of Ejector Nozzle Air Intake Design.

show the top view and side view, respectively, of the rocket flow path of a four clover configuration. The position and shape of the gate can be adjusted by manipulating any of the geometric variables shown. A complete list of the five variables to be optimized, and their corresponding bounds are given in Table 1. The bounds of the geometric variables define the outline of the search space. It should be noted that not all possible combinations of the geometric variables will produce a viable rocket flow path solution. For example, if the gate arc angle, ψ_g , is too small there will not be sufficient area for the rocket mass flow. Non-viable solutions are considered in the search space, however they are not assigned a fitness value in the same manner as viable solutions. The shaded area of Fig. 5 shows where viable solutions lie on a plane given by nondimensionalized gate radius, r_g/r_e , and gate depth, z_g/z_e . This plane represents two dimensions of the five dimensional search space. Note that in Table 1, r_e and z_e are defined by the user, and $\chi = 180/\varepsilon$.

2.2 Genetic Algorithm

The principle of optimization by genetic algorithm, developed by Holland [12], is used in the present study. A genetic algorithm is character-

Table 1 Nondimensional Geometric Variables

| Variable | Symbol | Bounds |
|-------------------|---------------|-------------------|
| Number of clovers | ε | $3 \rightarrow 6$ |
| Outlet arc angle | ψ_e/χ | $0 \rightarrow 1$ |
| Gate arc angle | ψ_g/χ | $0 \rightarrow 1$ |
| Gate depth | z_g/z_e | $0 \rightarrow 1$ |
| Gate radius | r_g/r_e | $0 \rightarrow 1$ |

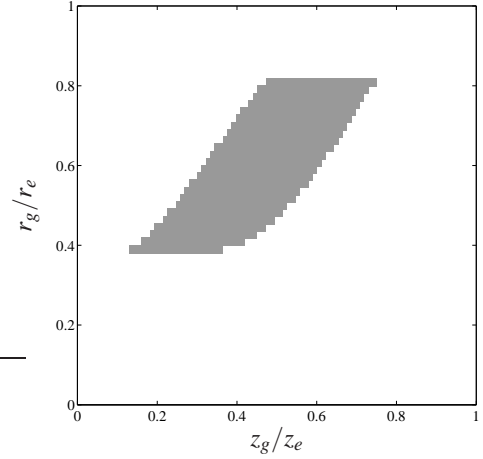


Fig. 5 Shaded Region Shows Viable Solutions On z_g/z_e - r_g/r_e Plane.

ized by the following components: a genetic representation of the solution, a population of solutions, an evaluation function, a fitness function, and genetic operators.

The five variables given in Table 1 represent the five genes that define an individual. An individual is expressed as

$$x_i^k = [x_{i,1}^k, x_{i,2}^k, \dots, x_{i,j}^k, \dots, x_{i,n}^k] \quad (1)$$

where k indicates the generation number, i is an arbitrary individual of the population, j is an arbitrary gene and n is the number of genes that defines an individual (for this work $n = 5$).

An initial population of individuals is required to begin the genetic algorithm. It has been suggested that larger population sizes show better performance (avoidance of local maxima), while smaller population sizes converge in a shorter period of time. A reasonable range for population size is 30–80 individuals [13]. The population is

expressed as

$$X^k = [x_1^k, x_2^k, \dots, x_i^k, \dots, x_m^k] \quad (2)$$

and m is the number of individuals in the population (for this work $m = 30$).

The fitness function defines a value by which all individuals are ranked. The optimal rocket flow path should have a high inlet area through which a high mass flow of atmospheric air will be entrained. The rocket flow path should also have smooth contours such that the flow within the nozzle remains close to isentropic. Additionally, the rocket flow path should have an exhaust profile that has a high shear layer area so that mixing with atmospheric air will be maximized. A fitness function that allows for the consideration of each of these criteria, and which can weigh them accordingly, is expressed by Eq. 3,

$$F = K_a \frac{A}{A_{max}} + K_b \left[1 - \left(\frac{|\phi - \phi_o|}{\phi_o} \right)^p \right] + K_c \frac{L}{L_{max}} \quad (3)$$

where K_a , K_b , and K_c are tunable weights. A is the calculated air intake area and $A_{max} = \pi r_e^2$. The variable ϕ is the angle through which the flow turns at the gate, while $\phi_o = 180^\circ$ is set as a desirable angle such that the flow within the rocket nozzle remains close to isentropic. L is the calculated exit arc length and $L_{max} = 2.1\pi r_e^2$. Finally, $p = 0.8$ is a penalty parameter used to control the rate at which the fitness of nozzles that show a difference between ϕ and ϕ_o is reduced. Table 2 shows the tunable weights of the fitness function that were simulated.

The genetic operators, used to alter the individuals at each progressive generation, are selection, cross-over, and mutation. The operators are tunable by adjusting the selection pressure, cross-over rate and mutation rate, respectively.

The selection operator is used to choose parents from the population. These parents are selected via the Roulette-Wheel method. Selection is random, however, more fit individuals have a higher probability of being selected. The probability of being selected is expressed by Eq. 4.

$$P(x_i^k) = \frac{F(x_i^k)^\sigma}{\sum_{u=1}^m F(x_u^k)^\sigma} \quad (4)$$

where σ is the selection pressure (for this work, an adaptive selection pressure is implemented where σ varies between 0.8 and 1). Given a population, X^1 , of 30 individuals, a set of parents selected for reproduction could be x_3^1 and x_{25}^1 . The population size is held constant for each generation, therefore, a total of 28 sets of parents are selected for reproduction and the remaining 2 children are selected by an elitist method. This method passes the top 2 most fit individuals to the following generation. This ensures that the GA will never diverge.

The cross-over operator is used to recombine the genetic information of both parents to produce a child. A non-traditional cross-over method is used in this work, where the recombination of real-parameter genes is accomplished one gene at a time. The cross-over rate is set at 60%, so that there is a 60% chance that the child will obtain the first gene from the more fit parent and a 60% chance that the child will obtain the second gene from the more fit parent, and so on. Using the previous example, and assuming that x_3^1 is more fit than x_{25}^1 , the child produced by these two parents could be $x_1^2 = [x_{3,1}^1, x_{25,2}^1, x_{3,3}^1, x_{3,4}^1, x_{25,5}^1]$. In other words, the first individual of the second generation will have received gene 1, 3, and 4 from the third individual of the first generation and gene 2 and 5 from 25th individual of the first generation.

Table 2 Parameters Of Fitness Function (Eq. 3)

| Case | K_a | K_b | K_c |
|------|-------|-------|-------|
| A | 1 | 0 | 0 |
| B | 0 | 1 | 0 |
| C | 0 | 0 | 1 |
| D | 0.4 | 0.3 | 0.3 |

The first two genetic operators, selection and cross-over, are capable of exploring the search space for an optimal solution. However, this search space is a limited subspace defined by all possible combinations of alleles that were present in the initial population (an allele is the numerical value of a particular real-parameter gene). In order to search the entire search space a genetic

operator that introduces new alleles into the population is required. For this purpose the mutation operator is used to create new alleles (for this work, an adaptive mutation rate is implemented where mutation rate varies between 10% and 50%). The new allele is randomly selected but remains within the bound for a given gene given in Table 1. Continuing the example, a gene of x_1^2 could be mutated such that the individual is now defined by a new set of alleles: $x_1^2 = [x_{3,1}^1, x_{25,2}^1, \widetilde{x_{3,3}^1}, x_{3,4}^1, x_{25,5}^1]$ where $\widetilde{x_{3,3}^1} = x_{3,3}^1 \pm \lambda$ (λ is a random mutation). A high mutation rate is not desirable since this would reduce the genetic algorithm to a random search algorithm.

3 Results and Discussion

3.1 Convergence of the GA

It is desirable for the GA to converge to the optimal solution in the shortest period of time. The convergence time will be a function of several factors. The most obvious is the dimension of the search space; a large search space should require more time to converge when compared with a small search space. Let Eq. 5 define the size of the search space,

$$S = \sum_{j=1}^n \frac{x_{i,j}^k |_{max} - x_{i,j}^k |_{min}}{\Delta x_{i,j}^k} \quad (5)$$

where $\Delta x_{i,j}^k$ is the step size used to discretize the j^{th} dimension of the search space. It is not immediately clear how the population size, mutation rate, cross-over rate, number of elites, or selection pressure will affect the convergence time. To make the GA as efficient as possible, sensitivity analyses are run to determine the best parameters for the genetic operators. A search space of $S = 100 \cdot 10^6$ is used throughout the analyses. The metric used to measure convergence time is the number of individuals that are evaluated while the algorithm converges ($\Gamma = m \cdot k$). Fig. 6 shows a histogram plot for several population sizes using a constant mutation rate of 10% and a constant selection pressure of 0.8. Fig. 7 shows a histogram plot for several population sizes using an

adaptive mutation rate and selection pressure. In each case the GA is allowed to reach convergence 100 times (i.e. the sum of all the bars for a given population size totals 100). In the adaptive technique, the mutation rate is switched between 10% and 50% based on the homogeneity of the population at a given generation. When the population is deemed to be too homogeneous, the mutation rate is increased to 50% in order to increase the diversity of the population. The selection pressure (σ) is switched between 0.8 and 1 based on trap situations. When the GA is deemed to be trapped in a local maximum, the selection pressure is increased to 1 in order to focus the search toward more fit solutions.

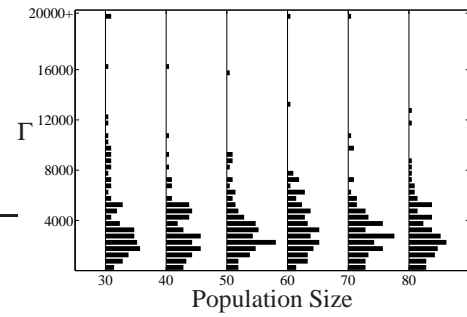


Fig. 6 Histogram Of Convergence Metric For Several Population Sizes Using Constant Mutation and Selection.

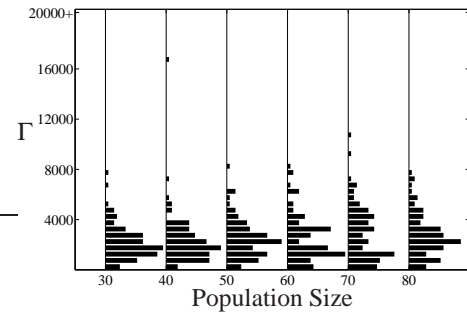


Fig. 7 Histogram Of Convergence Metric For Several Population Sizes Using Adaptive Mutation and Selection.

Comparing Fig. 6 and Fig. 7 it can be seen that a constant mutation rate and selection pressure is susceptible to trap situations. The bars in the $\Gamma = 20000+$ bin, indicating long convergence times, are indicative of trap situations. An adaptive mutation rate and selection pressure is

less likely to become trapped, as shown by the absence of bars in the higher bins of Fig. 7. It can also be seen that for each population size, the adaptive technique converges in a shorter period of time when compared with the constant parameter technique, as shown by the skewness of bars on Fig. 7 toward lower Γ values.

Comparing each population size of Fig. 7, it can be seen that a population size of 30 individuals is most skewed toward lower Γ values. For this reason, a population size of 30 was implemented for this work. Table 3 lists the parameters of the genetic operators that are used in the GA.

Table 3 Parameters Of The GA

| Parameter | Value |
|--------------------|------------------------|
| Population Size | 30 |
| Selection Pressure | 0.8 \rightarrow 1 |
| Crossover Rate | 60% |
| Mutation Rate | 10% \rightarrow 50 % |
| Number of Elites | 2 |

3.2 Optimized Rocket Flow Path

Varying the parameters of Eq. 3 will produce a unique optimal solution. In order to study the effect of various parameters, four cases were simulated, as given by Table 2. For test case A, the first term of Eq 3 is given 100% weight. Thus the GA produces a rocket flow path that is optimized for air intake area. Fig. 8(a) shows the convergence history of the most fit individual and the average fitness of the population at each generation. Convergence is reached within $k = 150$ generations, which corresponds to $\Gamma = 4500$. Referring to Fig. 7 it can be seen that this convergence metric falls within the expected range of $\Gamma < 8000$ for a population size of 30. Fig. 9(a) shows the optimized rocket flow path for case A. Although this solution has a high air intake area, $A = 0.67m^2$, which will lead to high entrainment of atmospheric air, it is expected that the low shear layer area of the rocket exhaust profile, which is related to the exit arc length, $L = 1.35m$, will not provide ideal mixing of the rocket and air stream.

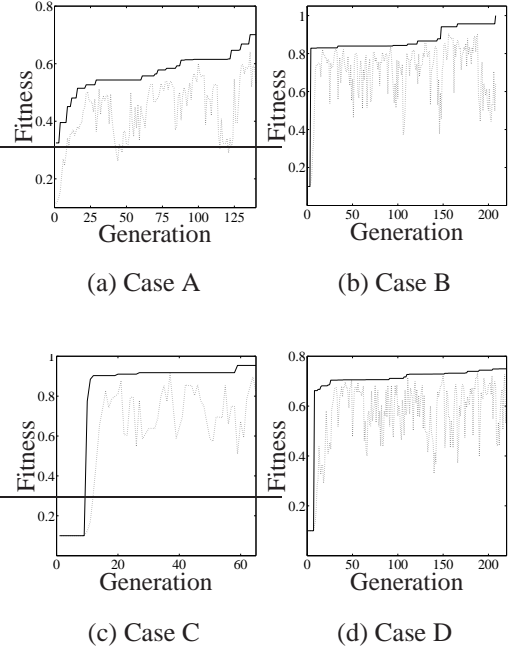


Fig. 8 Fitness Convergence History (Solid Line Represents Most Fit Solution, Dotted Line Represents Average Fitness Of Population).

For test case B, the second term of Eq 3 is given 100% weight. Thus the GA produces a rocket flow path that is optimized for flow turning angle. Fig. 8(b) shows the convergence history of the most fit individual and the average fitness of the population at each generation. Fig. 9(b) shows the optimized rocket flow path for case B. Although this solution has a desirable flow turning angle, $\phi = 180^\circ$, it is not an ideal rocket flow path for an ejector nozzle because the air intake area, $A = 0.52m^2$, and the exit arc length, $L = 1.68m$, are lower than desirable.

For test case C, the third term of Eq 3 is given 100% weight. Thus the GA produces a rocket flow path that is optimized for exit arc length. Fig. 8(c) shows the convergence history of the most fit individual and the average fitness of the population at each generation. Convergence is reached within $k = 60$ generations ($\Gamma = 1800$), which corresponds to the largest bar of Fig. 7 for a population size of 30 (i.e. the most likely convergence metric). Fig. 9(c) shows the optimized rocket flow path for case C. This solution has a high exit arc length, $L = 3.47m$, which creates an

essentially annular exhaust profile, however the low air intake area, $A = 0.46m^2$, suggests low entrainment of atmospheric air. Therefore, it is unlikely that this rocket flow path would be ideal for an ejector nozzle.

For test case D, all terms of Eq 3 are given nearly equal weight. Thus the GA produces a rocket flow path that is optimized for a combination of all three criteria. Fig. 8(d) shows the convergence history of the most fit individual and the average fitness of the population at each generation. Convergence is reached within $k = 250$ generations ($\Gamma = 7500$), which falls within the expected range of $\Gamma < 8000$ for a population size of 30. Fig. 9(d) shows the optimized rocket flow path for case D. This solution has a relatively high air intake area, $A = 0.57m^2$, and a high exit arc length, $L = 3.47m$. Thus, it is expected that this rocket flow path would be well suited for an ejector nozzle. Table 4 summarizes the results of the four test cases.

Table 4 Selection Criteria Of The Optimized Solutions.

| Case | ϵ | $A(m^2)$ | $\phi(deg)$ | $L(m)$ |
|------|------------|----------|-------------|--------|
| A | 4 | 0.67 | 174 | 1.35 |
| B | 5 | 0.52 | 180 | 1.68 |
| C | 6 | 0.46 | 151 | 3.47 |
| D | 6 | 0.57 | 127 | 3.47 |

The optimized rocket flow path of case D is used to design the air intake geometry of the ejector nozzle as described by [9]. Fig. 10(a) shows a 3D view of the air intake geometry. Fig. 10(b) shows a view frame view of the rocket flow path (dashed line) housed within the air intake geometry. This design represents the geometry of a potential RBCC engine upstream of the mixing duct. It can be seen that the cowl and fairings will affect the air intake area of the design. Therefore, future work will consider the air intake geometry in the fitness function.

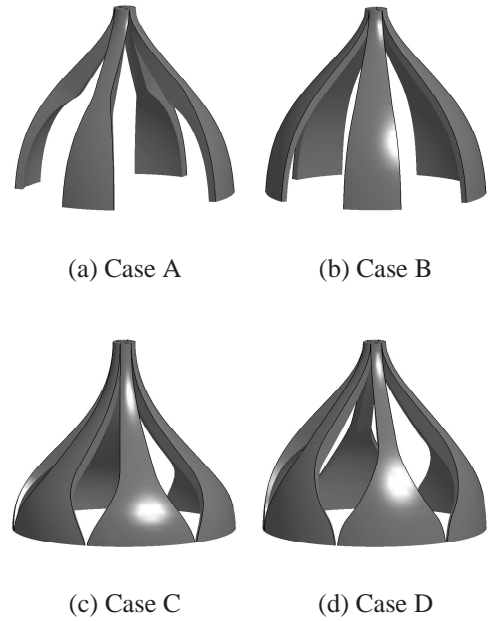


Fig. 9 Optimized Rocket Flow Path.

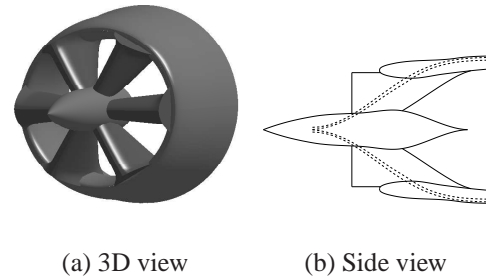


Fig. 10 Case D Optimal Ejector Nozzle Air Intake Design.

4 Conclusions

The implementation of a GA to determine the optimal rocket flow path configuration for a novel RBCC propulsion system is illustrated. The GA uses an adaptive mutation rate and selection pressure technique that shows better performance when compared with the standard technique of constant mutation rate and selection pressure. For the situations tested, the adaptive technique is able to avoid local traps and is able to converge in a shorter period of time.

The results show that the GA can produce a variety of rocket flow path solutions based on the user's selection of the tunable weights of the

fitness function. A nearly even balance of the tunable weights results in an optimal rocket flow path solution that will lead to high entrainment of atmospheric air and that should lead to good mixing of the rocket and air streams.

Future work will incorporate the geometric variables of the air intake geometry into the GA. Consideration will also be given to the design of the ejector engine as a whole, including the mixing duct downstream of the ejector nozzle.

5 Copyright Statement

The authors confirm that they, and/or their company or organization, hold copyright on all of the original material included in this paper. The authors also confirm that they have obtained permission, from the copyright holder of any third party material included in this paper, to publish it as part of their paper. The authors confirm that they give permission, or have obtained permission from the copyright holder of this paper, for the publication and distribution of this paper as part of the ICAS2010 proceedings or as individual off-prints from the proceedings.

References

- [1] Daines, R. L., Russell, R. M., *Numerical analysis of the effects of combustion in rocket ejectors*, AIAA 98-3772, July 1998.
- [2] Walker, J., Kamhawi, H., Krivanek, T., Thomas, S., Smith, T. D. *Status of the RBCC direct-connect mixer combustor experiment*, NASA/TM 2002-211555, May 2002.
- [3] Man, Z., Guo-qiang, H., Pei-jin, L., *Performance improved by multistaging rockets ejection in RBCC engine*, AIAA 2008-4504, July 2008.
- [4] Yungster, S., Trefny, C. J., *Analysis of a new rocket-based combined-cycle engine concept at low speed*, AIAA 99-2393, September 1999.
- [5] Russell, R. M., Brocco, D. S., Daines, R. L., *Modeling and validation of an ejector primary rocket for shielded afterburning fuel injection*, AIAA 1999-2241, June 1999.
- [6] Odegaard, E. A., Stroup, K. E., *1966 Advanced ramjet concepts program*, Volume III - Ejector Ramjet Engine Tests - Phase I, The Marquardt Corporation, Technical Report AFAPLTR- 67-118, January 1968.
- [7] Etele, J., Sislian, J. P., Parent, B., *Effect of rocket exhaust configurations on ejector performance in RBCC engines*, Journal of Propulsion and Power, Vol. 21, No. 4, pages 656-666, 2005.
- [8] Cerantola, D., Etele, J., *A nozzle concept to entrain atmospheric air for ejector operation*, AIAA 2006-8089, 2006.
- [9] Waung, T., Etele, J., *An ejector air intake design method for a novel RBCC rocket nozzle*, AIAA 2009-5294, 2009.
- [10] Zotes, F. A., Penas, M. S., *Multi-criteria genetic optimisation of the manoeuvres of a two-stage launcher*, Information Sciences: an International Journal, New York, NY, 2010, pp. 896-910.
- [11] Hwang, Shun-Fa, He, Rong-Song, *Improving real-parameter genetic algorithm with simulated annealing for engineering problems*, Advances in Engineering Software, Vol. 37, Issue 6, 2006, pp. 406-418.
- [12] Holland, J. H., *Adaption in natural and artificial systems*, The MIT Press, 1992.
- [13] De Jong, K. A., *Analysis of the behaviour of a class of genetic adaptive systems*, Technical Report No 185, University of Michigan, August 1975.